Solar Energy Materials & Solar Cells 101 (2012) 295–302

Contents lists available at SciVerse ScienceDirect

Solar Energy Materials & Solar Cells

journal homepage: www.elsevier.com/locate/solmat

Fabrication of OPVs by introducing a conductivity-enhanced hybrid buffer layer

Soo Won Heo [a], In Sung Song [b], Young Sung Kim [c], Doo Kyung Moon [a,*]

[a] Department of Materials Chemistry and Engineering, Konkuk University, 1 Hwayang-dong, Gwangjin-gu, Seoul 143-701, Republic of Korea
[b] Material & Device Laboratory, Corporation Technology Operations SAIT, Samsung Electronics, San #14-1 Nongseo-dong, Giheung-gu, Yongin-City, Gyunggi-do 446-712, Republic of Korea
[c] Graduate School of NID Fusing Technology, Seoul National University of Science & Technology, 138 Gongneung gil, Nowon-gu, Seoul 139-743, Republic of Korea

ARTICLE INFO

Article history:
Received 26 October 2011
Received in revised form
26 December 2011
Accepted 19 January 2012
Available online 7 March 2012

Keywords:
Organic photovoltaic cells (OPVs)
Au nanoparticles
Hybrid buffer layer
Hole mobility

ABSTRACT

Organic photovoltaic cells (OPVs) with a conductivity enhanced by doping with either dimethylsulfoxide (DMSO) or ethylene glycol (EG) were successfully fabricated to increase the photon harvesting property through localized surface plasmon resonance (LSPR) by adding Au nanoparticles to PH500, a hole collection layer, and effectively separating the generated charges. At Au nanoparticle and DMSO doping concentrations of 20 wt% and 1 wt%, respectively, the characteristics of the OPVs were optimized with a short-circuit current density (J_{sc}), open-circuit voltage (V_{oc}), fill factor (FF) and estimated power conversion efficiency (PCE) of 8.0 mA/cm^2, 0.595 V, 57.8% and 2.6%, respectively. Compared to the device with a buffer layer of conventional PEDOT:PSS, PCE was improved by ca. 85%. The series resistance (R_s), shunt resistance (R_{sh}), and hole mobility were 18 Ω cm^2, 673 Ω cm^2 and 4.2 cm^2/Vs, respectively.

1. Introduction

Thanks to their good mechanical properties and excellent electro-optical properties, π-conjugated polymers have attracted great attention as next-generation device materials for organic light-emitting diodes, organic thin-film transistors and organic photovoltaics (OPVs) [1–5]. In OPVs, in particular, solution processes such as screen printing [6], ink-jet printing [6], slot die coating [7], roll to roll stamping [8–11] and brush painting method [12,13] are applicable. Hence, low-cost, large-area, flexible and light weight devices can be fabricated.

At present, OPVs have a power conversion efficiency (PCE) of about 5% in the bulk-heterojunction system in which a photo active layer is formulated by blending the widely used donor material poly(3-hexylthiophene) (P3HT) with the acceptor material 6,6-phenyl-C61-butyric acid methyl ester [14]. One of the key issues in achieving high performance is sufficient photon absorption of the photoactive layer, i.e., efficient harvesting of sunlight. Nevertheless, the use of a thicker active layer inevitably increases the device resistance because of the low carrier mobilities of organic materials [15,16]. Therefore, the exploitation of localized surface plasmon resonance (LSPR) could be a solution to enhance light absorption without changing the film thickness [17,18]. The excitation of LSPR through the resonant interaction between the electromagnetic field of incident light and the surface electron density surrounding metallic nanoparticles causes local enhancement in the electromagnetic field, which is expected to enhance light harvesting in OPV devices [19,20].

Recently, hybrid-type OPVs have been fabricated by introducing metal nano compounds (e.g., PbSe, ZnO, $CuInS_2$, etc.) to the photo active layer in a particle, nano-rod or nano-dot form. However, a very low PCE of around 2% was observed [21–23]. In addition, Chen et al. reported the fabrication of OPVs with an active layer area of 0.12 cm^2 and PCE of 4.19% by introducing the Au nano particle-doped buffer layer to poly(3,4-ethylene dioxythiophene):poly(styrene sulfonate) (PEDOT:PSS) [24]. As shown above, most studies have focused on improving the improvement of the photon harvesting property by introducing metal nanoparticles to the buffer layer or photo active layer. The improvement of photon harvesting property through LSPR has facilitated the generation of many holes and electrons. However, because of the low conductivity of the polymer or buffer layer, the separated holes and electrons were recombined without flowing out through the external circuit.

In this study, therefore, the photon harvesting property is enhanced by introducing an Au nanoparticle-doped hybrid buffer layer in the buffer layer (i.e., hole collection layer). In addition, OPVs in which the conductivity of the hybrid buffer layer has been enhanced are fabricated to effectively separate the generated charges and prevent them from being recombined before flowing

* Corresponding author. Tel.: +82 2 450 3498; fax: +82 2 444 0765.
E-mail address: dkmoon@konkuk.ac.kr (D.K. Moon).

0927-0248/$ - see front matter © 2012 Elsevier B.V. All rights reserved.
doi:10.1016/j.solmat.2012.01.027

out through the external circuit. For a buffer layer, the modified PEDOT:PSS (PH500) is used. Then, the harvesting property of the photons is enhanced by optimizing the Au nanoparticle doping concentration. To improve the conductivity of the hybrid buffer layer, moreover, dimethylsulfoxide (DMSO) and ethylene glycol (EG) are added at various concentrations for optimization. As a result, OPVs are fabricated and their surfaces are observed through atomic force microscopy (AFM). Finally, the current density–voltage (J–V) characteristics and the incident photon-to-current conversion efficiency (IPCE) of the resultant photovoltaic device are measured.

2. Materials and measurements

2.1. Materials

Conventional PEDOT:PSS (AI 4083) and modified PEDOT:PSS (PH 500) were purchased from Clevios. DMSO and EG, which were used to enhance the conductivity of PH500, were purchased from Aldrich. P3HT, a donor material in the photo active layer, was purchased from Rieke Metals while the acceptor material $PC_{61}BM$ was bought from Nano C. Au nanoparticles were synthesized in accordance with the method mentioned in the literature [25].

2.2. Measurements

All thin films were fabricated using a GMC2 spin coater (Gensys), and the thickness was measured with an alpha step 500 surface profiler (KLA-Tencor). The surface plasmon resonance (SPR) absorption band and nanocrystal image were measured with UV–vis spectroscopy (HP Agilent 8453) and field mission scanning electron microscopy (FE-SEM, JEOL JSM-6701F), respectively, by determining the size of the synthesized Au nanoparticles. X-ray diffraction (XRD) patterns were observed using a Rigaku D/MAX 2200 diffractometer with Cu Kα radiation. The electrical properties of the hybrid buffer layer were measured using a 4-point probe station (MST6000C). The surface of the fabricated device was observed through AFM (PSIA XE-150) and FE-SEM. The J–V characteristics of the OPVs were measured using a Keithley 2400 source measure unit. The devices were evaluated at 298 K in air using a Class A Oriel solar simulator (Oriel 96000 150W solar simulator) having an xenon lamp that simulates AM 1.5G irradiation (100 mw/cm^2) from 400 to 1100 nm. The instrument was calibrated with a monocrystalline Si diode fitted with a KG5 filter to bring the spectral mismatch to unity. The calibration standard was calibrated by the National Renewable Energy Laboratory (NREL). IPCE (Mc science) was measured against the best performance device at 298 K in air.

3. Experimental part

3.1. Cleaning of ITO glass and bare glass

To clean the indium tin oxide (ITO) glass (10 Ω/sq, Samsung corning) and bare glass, detergent (Alconox® in deionized water, 10%), acetone, isopropyl alcohol and deionized water were each sonicated in order for 20 min. The moisture was removed by blowing thoroughly with N_2 gas. To ensure complete removal of all of the remaining water, the ITO glass and bare glass were baked on a hot plate for 10 min at 100 °C. For hydrophilic treatment of the ITO glass and bare glass surface, they were cleaned for 10 min in a UVO cleaner.

3.2. Synthesis of Au nanoparticles

The Au nanoparticles used in this study were synthesized in accordance with the method mentioned in the literature [25]. During the synthesis, the SPR absorption band according to particle size was measured through UV–vis spectroscopy. In addition, the size and shape of the Au nanoparticles were observed through FE-SEM, and the crystal structure of the Au nanoparticles was analyzed through XRD patterns. The study results are shown in the Supporting Information (SI) in Figs. S1 to S3.

3.3. Formulation of buffer layer ink and fabrication of buffer layers

To measure the electrical properties of conventional PEDOT:PSS (AI 4083) and modified PEDOT:PSS (PH 500), they were spin-coated at 1000 rpm on a cleaned bare glass and annealed at 120 °C for 20 min. The electrical properties of the thin films thus fabricated were measured using a 4-point probe station. To measure the electrical properties of PH500 according to the Au nanoparticle doping concentration, Au nanoparticle solution (0.1 mg/ml) (~50 nm size) was doped at 10, 20 and 30 wt%. Then, a hybrid buffer layer ink was formulated and its conductivity was increased by doping with DMSO and EG at 0.5, 1.0 and 3.0 wt%. To observe the electrical properties, surface morphology and distribution of Au nanocrystals of the resulting conductivity-enhanced hybrid buffer layer, the solutions were spin-coated at 1000 rpm in a cleaned bare glass and annealed at 120 °C for 20 min. The characteristics of the fabricated thin films were measured through a 4-point probe station and AFM.

3.4. Fabrication of OPVs

3.4.1. Optimization of the Au nanoparticle doping concentration

To effectively harvest photons through LSPR, the concentration of Au nanoparticles that were doped in the buffer layer was optimized. As shown in Fig. 1, OPVs with a conductivity-enhanced hybrid buffer layer were fabricated. All manufacturing processes of the devices were performed in the glove box. After spin-coating conventional PEDOT:PSS in which Au nanoparticles were doped on the patterned ITO glass at 10, 20 and 30 wt%, a 40 nm-thick hybrid buffer layer was formed. Then, solutions were annealed on the hot plate at 120 °C for 20 min to remove any residual solvents. The solutions, which were blended with an ortho-dichlorobenzene (ODCB) concentration of 1.5 wt% and a P3HT/$PC_{61}BM$ ratio of 1:0.6 for a photo active layer were spin-coated at 500 rpm on the hybrid buffer layer to form a 130 nm-thick layer and then annealed at 160 °C for 10 min. To form the cathode, BaF_2 (0.1 Å/s, 2 nm), Ba (0.2 Å/s, 2 nm) and Al (5 Å/s, 100 nm) were thermally deposited in order in a high-vacuum chamber. Finally, OPVs with an active area of 225 mm^2 (15 mm × 15 mm) were fabricated through encapsulation.

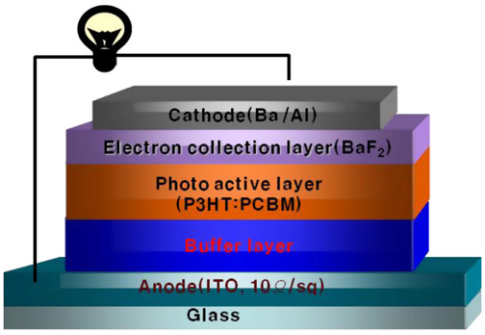

Fig. 1. Device structure of OPV in this study.

3.4.2. Optimization of the doping concentration of DMSO and EG

To optimized the doping concentration of DMSO and EG for maximizing the conductivity of PH500, OPVs featuring a conductivity-enhanced hybrid buffer layer were fabricated, as shown in Fig. 1. The fabrication condition of the OPVs was the same as that described above in Section 3.4.1, except that the concentration of Au nanoparticles and crystalline size were set at 20 wt% and ~50 nm, respectively. Then, the concentrations of the doped DMSO and EG were both set to 0.5, 1.0 and 3.0 wt%.

4. Results and discussion

Table 1 shows conventional PEDOT:PSS, PH 500 and the electrical properties of the thin films in which Au nanoparticles were doped at 10, 20 and 30 wt%. The conductivity of pristine PEDOT:PSS and pristine PH500 was 2.3×10^{-4} S/cm and 0.15 S/cm, respectively. However, when Au nanoparticles were doped at 20 wt%, the conductivity of both samples increased to 4.2×10^{-4} S/cm and 0.45 S/cm, respectively. In the case of PH500, in particular, the Au

Table 1
Electrical properties of hybrid buffer layers at various Au nanoparticle concentrations.

	Conventional PEDOT:PSS (AI 4083)				Modified PEDOT:PSS (PH 500)			
Au NPs concentrations[a] [wt%]	0	10	20	30	0	10	20	30
Resistivity [Ω cm]	4221	3030	2380	4000	6.32	4.75	2.22	3.33
Conductivity [S/cm]	0.00023	0.00033	0.00042	0.00025	0.15	0.21	0.45	0.30

Buffer layer thickness: 100nm, annealing: 20 min at 120 °C.

[a] Au nanoparticles crystalline size: ~50 nm, Au nanoparticles solution: 0.1 mg/ml.

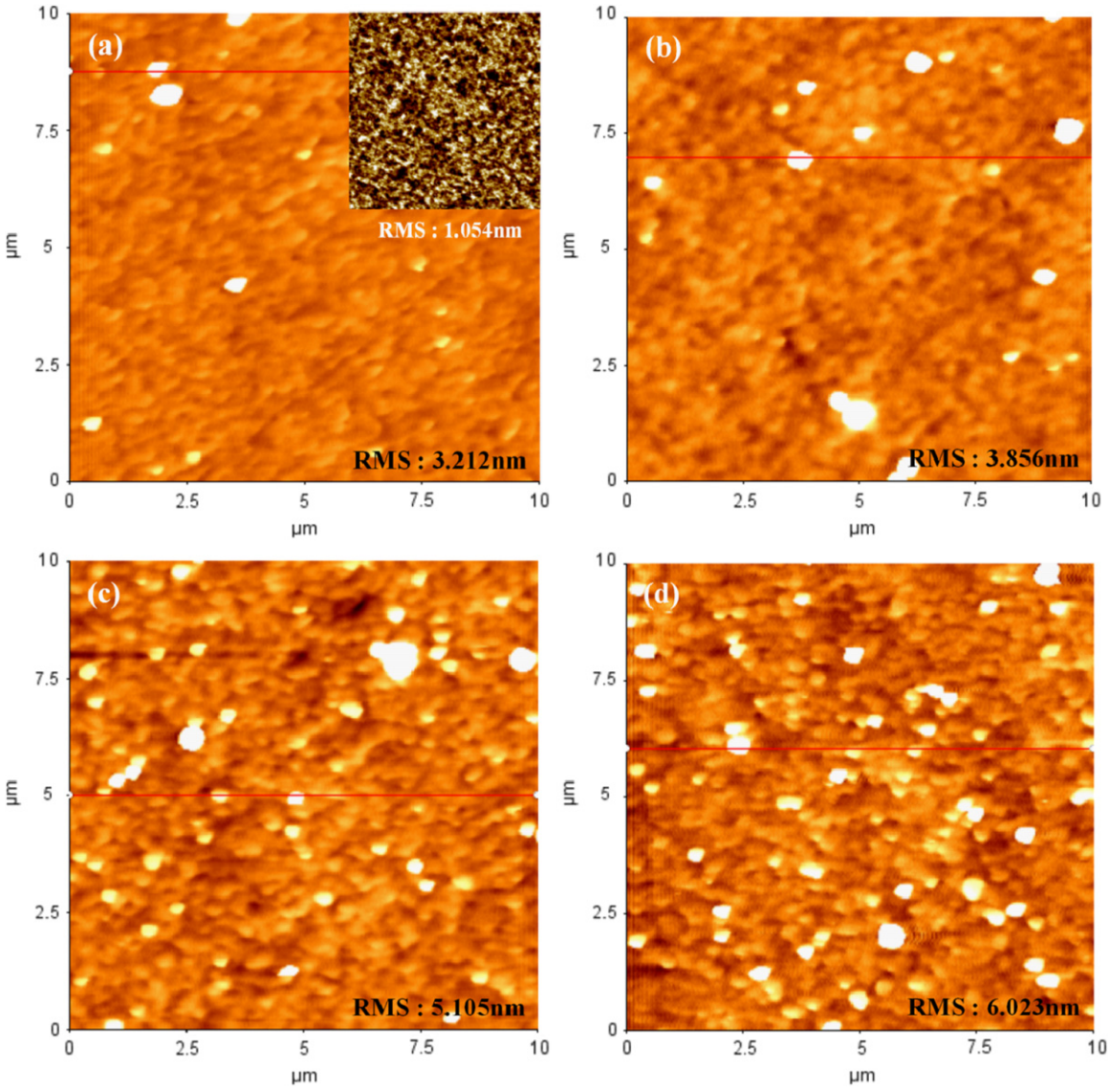

Fig. 2. AFM images of (a) PH 500 (inset, PEDOT:PSS), (b) PH 500+Au nanoparticles 10 wt%, (c) PH 500+Au nanoparticles 20 wt%, (d) PH 500+Au nanoparticles 30 wt%.

nanoparticle doping increased the conductivity three times. This increase was caused by the increase in surface electron density due to the strong electromagnetic field around metal nanoparticles after resonant interaction between the electromagnetic field of incident light and the electron density around the metallic nanoparticles [19]. Therefore, both the harvesting property and photon conductivity could be improved by the doping of Au nanoparticles in the buffer layer.

However, when the Au nanoparticle doping concentration was increased to 30 wt%, the conductivity decreased. As shown in Fig. 2(b) to (d), the increase in the Au nanoparticle doping concentration from 20 wt% to 30 wt% afforded poor thin film morphology, with the root mean square (RMS) roughness increasing from 3.865 nm to 6.023 nm. Therefore, the conductivity decreased due to the increase in RMS at the Au nanoparticle doping concentration of 30 wt%. As shown in Fig. 2(a), the RMS of pristine PH500 was greater than that of pristine PEDOT:PSS (Fig. 2(a) inset) because PEDOT was agglomerated. In PH500, the conductivity improved as PEDOT with high conductivity was partially agglomerated, but the morphology was degraded. Therefore, the RMS of PH500 was greater than that of PEDOT:PSS, but it also had high conductivity.

Even though the conductivity was slightly increased by the doped Au nanoparticles, it needs to be further enhanced to effectively separate the generated holes and electrons without recombination. Therefore, to enhance the conductivity, a hybrid buffer layer was fabricated by doping the PH500 containing 10–30 wt% of Au nanoparticles with DMSO or EG at 0.5–3.0 wt%. The results of the electrical property measurements are shown in Table 2 below.

The polar solvents with high-dielectric constants such as DMSO increased the conductivity of PEDOT:PSS by reducing the Coulombic interactions between the counter ion and charge carrier through the screen effect, which is strong between the positively charged PEDOT and the negatively charged PSS dopant. [26,27] Therefore, as the DMSO or EG doping concentration increased, the conductivity of the hybrid buffer layers was increased. At this time, a maximum conductivity of the hybrid buffer layer to a maximum at a DMSO or EG doping concentration of 3.0 wt%. As shown in Figs. 3 and 4, however, in the PH500 with Au nanoparticle concentration of 20 wt%, when the doping concentration of DMSO or EG was increased, the agglomerated PEDOT, which was as large as Au nanoparticles increased. In addition, the morphology of the thin films was degraded. Consequently, the conductivity in the thin films with a concentration of DMSO or EG and Au nanoparticles of 3.0 and 20 wt%, respectively, was maximized at 333 S/cm and 325 S/cm, respectively.

OPVs were fabricated to confirm the improvement of photon harvesting properties in a buffer layer after the introduction of Au nanoparticles, to increase the photovoltaic properties via the improved conductivity after doping with DMSO or EG, and to optimize the fabrication conditions. Various types of buffer layer ink formulated in the cleaned ITO glass were spin-coated to a thickness of 40 nm, and annealed at 120 °C for 20 min. The solutions, which were blended in ODCB at a concentration of 1.5 wt% with a P3HT/$PC_{61}BM$ ratio of 1:0.6 for a photo active layer were spin-coated on the hybrid buffer layer to form a 130 nm-thick layer and then annealed at 160 °C for 10 min. To form the cathode on the photo-active layer, lastly, BaF_2 (0.1 Å/s, 2 nm), Ba (0.2 Å/s, 2 nm) and Al (5 Å/s, 200 nm) were thermally deposited in a high vacuum chamber (1×10^{-6} Torr or less). BaF_2 was applied as an electron transporting layer to effectively collect the electrons through an Ohmic contact between the photo-active layer and the cathode. In addition, Ba (-2.7eV), a low work function material, was used as the cathode. A 100 nm-thick layer of Al was deposited to protect the cathode.

To compare the OPV performances according to the buffer layer conductivity, OPVs with a buffer layer of pristine PEDOT:PSS

Table 2
Electrical properties of conductivity-enhanced hybrid buffer layers at various concentrations of Au nanoparticles, DMSO and EG.

Additives concentrations [wt%]	Conductivity enhanced hybrid buffer layers																			
	DMSO									EG										
	0.5		1.0			3.0				0.5			1.0			3.0				
Au NPs concentrations[a] [wt%]	10	20	30	10	20	30	10	20	30	10	20	30	10	20	30	10	20	30	10	20	30
Resistivity [Ω cm]	0.120	0.054	0.064	0.049	0.022	0.027	0.0036	0.0030	0.0034	4.34	0.81	1.02	1.40	0.45	0.79	0.0053	0.0031	0.0042		
Conductivity [S/cm]	8.3	18.5	15.4	20	44.5	36	276	333	294	0.23	1.23	0.98	0.71	2.22	1.25	188	325	237		

Buffer layer thickness: 100 nm, annealing: 20 min at 120 °C.
[a] Au nanoparticles crystalline size: ~50 nm, Au nanoparticles solution: 0.1 mg/ml.

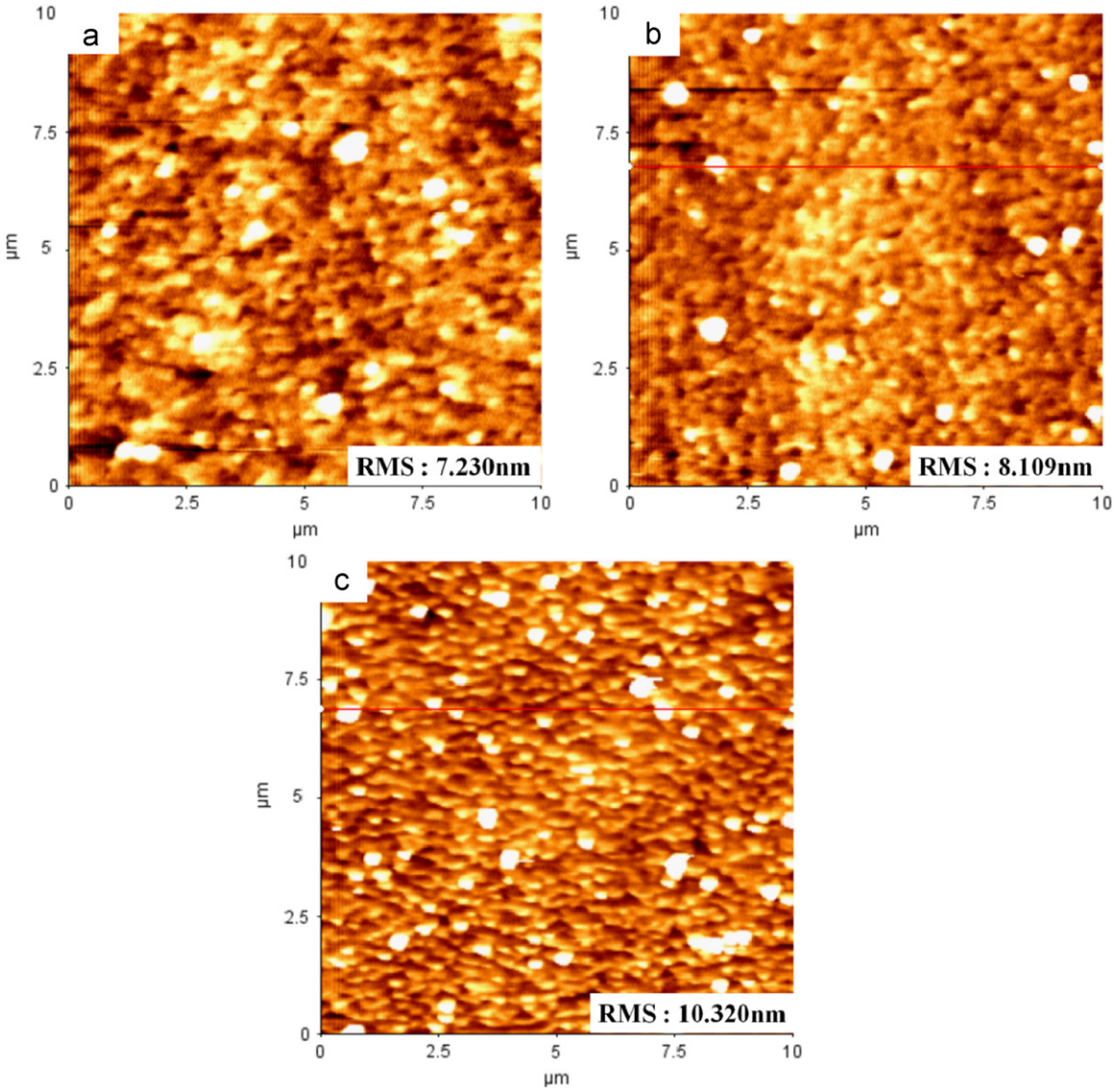

Fig. 3. AFM images of (a) PH 500+Au nanoparticles 20 wt%+DMSO 0.5 wt%, (b) PH 500+Au nanoparticles 20 wt%+DMSO 1.0 wt%, (c) PH 500+Au nanoparticles 20 wt%+DMSO 3.0 wt%.

or PH 500 were fabricated. As shown in Fig. 5 and Table 3, the pristine PEDOT:PSS-buffer layer device exhibited a PCE of 1.4%. In the pristine PH500-buffer layer device, PCE was increased to 1.6% due to the increase in current density from 6.6 to 7.3 mA/cm^2. However, the series resistance (R_s) was slightly increased from 43.36 to 45.19 Ω cm^2 due to the increase in internal resistance resulting from the poorer morphology of the PH500 layer (RMS=3.212 nm) compared to the PEDOT:PSS layer (RMS=1.054 nm). Therefore, the increased R_s was attributed to the rougher surface morphology. However, the shunt resistance (R_{sh}) increased from 243 to 252 Ω cm^2 due to the increase in carrier mobility caused by improved conductivity. Hence, the generated holes and electrons were well separated from each other, which in turn decreased the recombination probability. In addition, PCE was improved due to the increased current density.

A test was performed to compare the photon harvesting properties according to the concentration of Au nanoparticles doped in the buffer layer. To minimize the effect of conductivity, pristine PEDOT:PSS with low conductivity was used as the buffer layer. A hybrid buffer layer ink was formulated after adding 10–30 wt% of Au nanoparticles to the pristine PEDOT:PSS. The properties of the OPVs were fabricated using the ink were assessed. As shown in Fig. 5 and Table 3, at the Au nanoparticle doping concentration of 20 wt%, PCE was maximized at 1.7% with a short-circuit current density (J_{sc}) of 8.0 mA/cm^2. This PCE was 21% greater than the 1.4% PCE of the PEDOT:PSS-buffer layer device. Despite the almost unchanged open-circuit voltage (V_{oc}) and fill factor (FF), PCE was increased as a result of the increase in J_{sc} from 6.6 to 8.0 mA/cm^2 that was caused by the increased light absorption due to effect of LSPR and not the increased conductivity (Fig. 6).

As shown in Tables 1 and 3, the conductivity of the hybrid buffer layer (4.2×10^{-4} S/cm) was about 3 orders of magnitude lower than that of PH500 (0.15 S/cm), but the J_{sc} value of the former (8.0 mA/cm^2) was slightly higher than that of the latter. This higher J_{sc} value was caused by the increase in photon harvesting properties due to the doping of Au nanoparticles. Therefore, the current density has increased due to the decrease in internal resistance in the OPV with doped Au nanoparticles. In addition, R_s was decreased from 43.36 to 30.49 Ω cm^2. Nevertheless, PCE was not further increased because the separated holes and electrons were recombined due to the decrease in R_{sh} after the low conductivity of the hybrid buffer layer. Therefore, it was considered that the photon harvesting properties

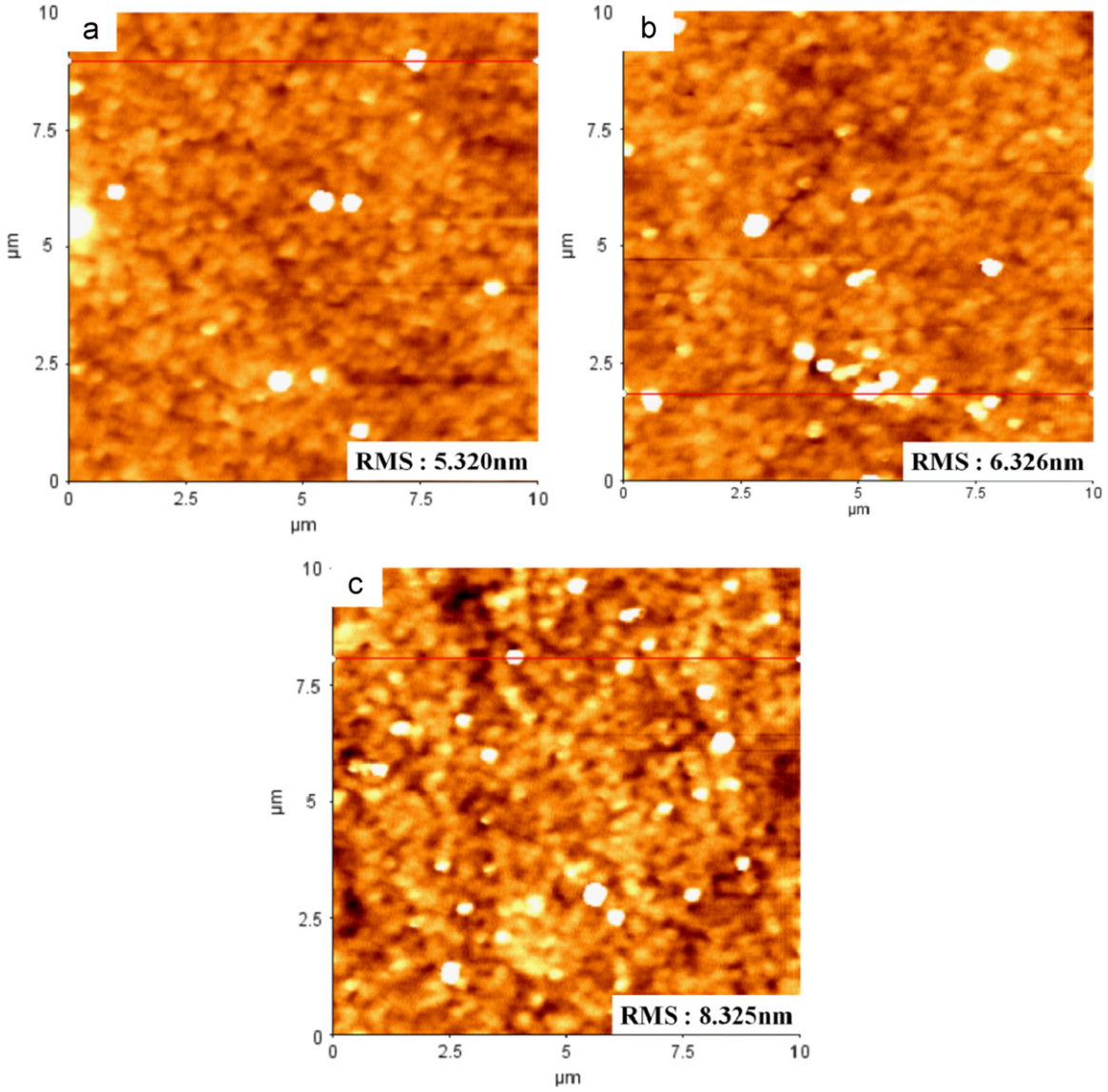

Fig. 4. AFM images of (a) PH 500+Au nanoparticles 20 wt%+EG 0.5 wt%, (b) PH 500+Au nanoparticles 20 wt%+EG 1.0 wt%, (c) PH 500+Au nanoparticles 20 wt%+EG 3.0 wt%.

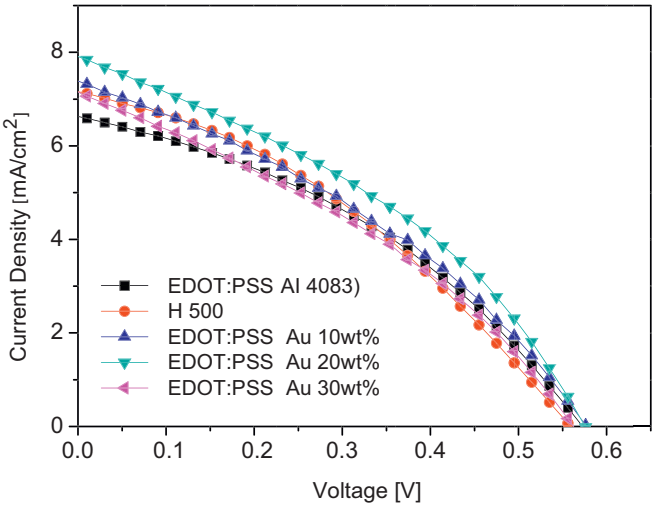

Fig. 5. *J–V* characteristics of the OPVs at various concentrations of Au nanoparticles in PEDOT:PSS layer.

could be enhanced by doping with Au nanoparticles, and that the OPV efficiency could also be improved through the increased conductivity in the buffer layer. After setting the doping level of Au nanoparticles to the optimal level (20 wt%) and doping with DMSO or EG in PH500 in order to maximize the conductivity, the properties of the OPVs with the fabricated conductivity-enhanced hybrid buffer layer were assessed. The doping levels of DMSO and EG were both 0.5, 1.0 and 3.0 wt%.

The *J–V* characteristics of the OPVs that were fabricated in accordance with the doping level of DMSO or EG are shown in Support Information, along with the IPCE data (Fig. S4). As shown in Fig. 7(a) and Table 3, PCE was maximized at 2.6% and 2.2% at DMSO and EG doping concentrations of 1.0 wt%, respectively. In the IPCE data in Fig. 7(b), the pristine PEDOT:PSS device exhibited an external quantum efficiency (EQE) of 28.8% (λ_{max}=490 nm). In OPVs with DMSO and EG doping concentrations of 1.0 wt%, EQE was increased to 36.7% (λ_{max}=540 nm) and 34.2% (λ_{max}=500 nm), respectively. In the former OPV, the V_{oc} value (0.595 V) was the same as that of PH500, and was slightly increased from that of PEDOT:PSS (0.575 V), J_{sc} and FF were increased from 6.6 to 8.0 mA/cm^2 and from 37.6% to

Table 3
Characteristics of devices.

Buffer layers	J_{sc} [mA/cm^2]	V_{oc} [V]	FF [%]	PCE [%]	Series resistance [Ω cm^2]	Shunt resistance [Ω cm^2]
PEDOT:PSS(AI 4083)	6.6	0.575	37.6	1.4	43.36	243
PH 500	7.3	0.595	37.3	1.6	45.19	252
PEDOT:PSS						
Au 10 wt%	7.3	0.575	35.4	1.5	37.31	150
Au 20 wt%	8.0	0.575	36.2	1.7	30.49	158
Au 30 wt%	7.1	0.555	35.1	1.4	36.94	123
PH 500+Au 20 wt%						
DMSO 0.5 wt%	6.8	0.595	48.5	2.0	30.44	460
DMSO 1.0 wt%	8.0	0.595	57.8	2.6	18.08	673
DMSO 3.0 wt%	7.9	0.595	50.9	2.4	25.96	235
EG 0.5 wt%	7.8	0.595	44.2	2.0	25.92	252
EG 1.0 wt%	7.9	0.595	47.5	2.2	24.67	367
EG 3.0 wt%	7.6	0.595	45.7	2.1	24.53	359

ITO/buffer layers/P3HT:PCBM(1:0.6)/BaF_2/Ba/Al.

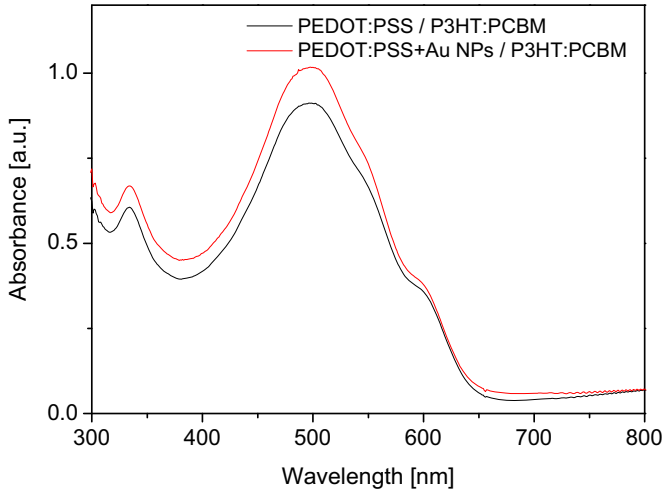

Fig. 6. UV–vis absorption spectra at PEDOT:PSS/P3HT:PCBM bilayer with/without Au nanoparticles in PEDOT:PSS.

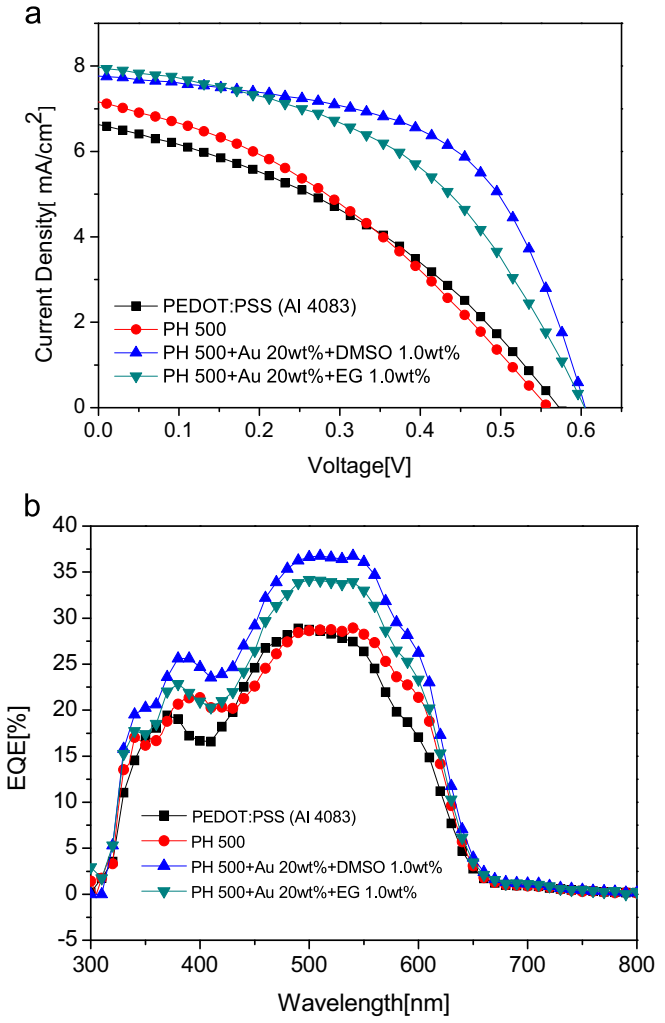

Fig. 7. (a) *J–V* characteristics of the OPVs for various modified buffer layers, (b) IPCE data of fabricated devices for various modified buffer layers.

57.8%, respectively. PCE was increased by 85% to 2.6% compared to the PEDOT:PSS device with a PCE of 1.4%.

Charge mobility study of the devices with PEDOT:PSS and conductivity-enhanced hybrid buffer layer as hole collection layer was conducted with hole-only devices using the space charge limited current (SCLC) methods [28–30]. The configuration of hole-only devices and graphs of the logarithm of JL^3/V^2 versus the square root of the mean electric field are shown in Fig. S5. The hole mobility of the device with PEDOT:PSS layer was calculated to be 3.8×10^{-2} cm^2/Vs, whereas the device with conductivity-enhanced hybrid buffer layer had a value as high as 4.2 cm^2/Vs. The hole mobility was about 2 orders of magnitude higher than that of the device with PEDOT:PSS layer. Because of the high hole mobility of the device with conductivity-enhanced hybrid buffer layer, therefore, J_{sc} and FF were increased from 6.6 to 8.0 mA/cm^2 and from 37.6% to 57.8%, respectively.

As R_s was decreased from 43.36 to 18.08 Ω cm^2, the photocurrent was increased due to the LSPR effect, the conductivity was improved due to addition of DMSO, and the internal resistance was therefore decreased. In particular, R_{sh} was increased from 243 to 673 Ω cm^2, which decreased the charge recombination between the buffer layer and the photo active layer interface, and therefore increased FF by over 53%. The introduction of a conductivity-enhanced hybrid buffer layer decreased R_s but increased hole mobility and R_{sh}. As a result, both J_{sc} and FF increased, which in turn enhanced PCE. Even though the conductivity of the buffer layer was increased when DMSO was doped at 3.0 wt%, RMS was increased from 8.10 to 10.32 nm due to the increase in agglomerated PEDOT, as shown in Fig. 3. The increase in RMS had no impact on the changes in J_{sc}, but decreased FF from 57.8 to 50.9% due to the decrease in R_{sh} from 673 to 235 Ω cm^2. As a result, the charge recombination between the buffer layer and the photo active layer interface was increased.

Compared to the PEDOT:PSS device, PCE was increased by 57% to 2.2% in the device with 1.0 wt% of EG. However, it was less efficient than the DMSO-featured device. As shown in Fig. 4(b), 1.0 wt% of EG was added to PH500 with an Au nanoparticle doping concentration of 20 wt%. The RMS of the thin film (6.436 nm) was lower than that (8.109 nm) of the thin film with 1.0 wt% of DMSO. However, the former thin film showed low conductivity (2.22 S/cm). Even though the EG doping level was increased to enhance the conductivity, the morphology of the thin film slightly degraded, which decreased PCE.

5. Conclusion

In this study, OPVs with a conductivity that was enhanced by doping with DMSO or EG were successfully fabricated to improve

the photon harvesting properties through LSPR by adding Au nanoparticles to a buffer layer of PH500 and effectively separating the generated charges. At Au nanoparticle and DMSO doping concentrations of 20 and 1.0 wt%, respectively, the OPV properties were optimized at PCE of 2.6%, J_{sc} of 8.0 mA/cm^2, V_{oc} of 0.595 V and FF of 57.8%. The Au nanoparticle and DMSO doping in buffer layer increased hole mobility. Therefore, R_s was decreased from 43.36 to 18.18 Ω cm^2, which decreased the internal resistance of the device. In addition, the charge recombination between the buffer layer and the photo active layer interface was decreased due to the increase in R_{sh} from 243 to 673 Ω cm^2. Consequently, PCE was increased by ca. 85% compared to the device with conventional PEDOT:PSS as a buffer layer.

Acknowledgment

This research was supported by a grant (10037195) from the Fundamental R&D Program for Core Technology of Materials funded by the Ministry of Knowledge Economy, Republic of Korea and the National Research Foundation of Korea Grant funded by the Korean Government (MEST) (NRF-2009-C1AAA001-2009-0093526)

Appendix A. Supporting materials

Supplementary data associated with this article can be found in the online version at doi:10.1016/j.solmat.2012.01.027.

References

[1] S.O. Jeon, J.Y. Lee, Improved high temperature stability of organic solar cells using a phosphine oxide type cathode modification layer, Solar Energy Materials and Solar Cells 95 (2011) 1102–1106.
[2] J.Y. Lee, W.S. Shin, J.R. Haw, D.K. Moon, Low band-gap polymers based on quinoxaline derivatives and fused thiophene as donor materials for high efficiency bulk-heterojunction photovoltaic cells, Journal of Materials Chemistry 19 (2009) 4938–4945.
[3] J.Y. Lee, S.W. Heo, H. Choi, Y.J. Kwon, J.R. Haw, D.K. Moon, Synthesis and characterization of 2,1,3-benzothiadiazole-thieno [3,2-b] thiophene-based charge transferred-type polymers for photovoltaic application, Solar Energy Materials and Solar Cells 93 (2009) 1932–1938.
[4] J.Y. Lee, M.H. Choi, S.W. Heo, D.K. Moon, Synthesis of random copolymers based on 3-hexylthiophene and quinoxaline derivative: Influence between the intramolecular charge transfer (ICT) effect and π-conjugation length for their photovoltaic properties, Synthetic Metals 161 (2011) 1–6.
[5] J.Y. Lee, M.H. Choi, H.J. Song, D.K. Moon, Random copolymers based on 3-hexylthiophene and benzothiadiazole with induced π-conjugation length and enhanced open-circuit voltage property for organic photovoltaics, Journal of Polymer Science Part A: Polymer Chemistry 48 (2010) 4875–4883.
[6] F.C. Krebs, Fabrication and processing of polymer solar cells: a review of printing and coating techniques, Solar Energy Materials and Solar Cells 93 (2009) 394–412.
[7] J. Alstrup, M. Jørgensen, A.J. Medford, F.C. Krebs, Ultra fast and parsimonious materials screening for polymer solar cells using differentially pumped slot-die coating, ACS Applied Materials & Interfaces 2 (2010) 2819–2827.
[8] E. Bundgaard, O. Hagemann, M. Manceau, M. Jørgensen, F.C. Krebs, Low band gap polymers for roll-to-roll coated polymer solar cells, Macromolecules 43 (2010) 8115–8120.
[9] M. Manceau, D. Angmo, M. Jørgensen, F.C. Krebs, ITO-free flexible polymer solar cells: from small model devices to roll-to-roll processed large modules, Organic Electronics 12 (2011) 566–574.
[10] F.C. Krebs, J. Fyenbob, M. Jørgensen, Product integration of compact roll-to-roll processed polymer solar cell modules: methods and manufacture using flexographic printing, slot-die coating and rotary screen printing, Journal of Materials Chemistry 20 (2010) 8994–9001.
[11] F.C. Krebs, Roll-to-roll processing and product integration of polymer solar cells, Energy & Environmental Science 3 (2010) 512–525.
[12] S.W. Heo, J.Y. Lee, H.J. Song, J.R. Ku, D.K. Moon, Patternable brush painting process for fabrication of flexible polymer solar cells, Solar Energy Materials and Solar Cells 95 (2011) 3041–3046.
[13] S.W. Heo, K.W. Song, M.H. Choi, T.H. Sung, D.K. Moon, Patternable solution process for fabrication of flexible polymer solar cells using PDMS, Solar Energy Materials and Solar Cells (2011) 3564–3572.
[14] C.J. Ko, Y.K. Lin, F.C. Chen, C.W. Chu, Modified buffer layers for polymer photovoltaic devices, Applied Physics Letters 90 (2007). (063509-1–063509-3).
[15] V. Shrotriya, E.H.E. Wu, G. Li, Y. Yao, Y. Yang, Efficient light harvesting in multiple-device stacked structure for polymer solar cells, Applied Physics Letters 88 (2006). (064104-1–064104-3).
[16] A. Yakimov, S.R. Forrest, High photovoltage multiple-heterojunction organic solar cells incorporating interfacial metallic nanoclusters, Applied Physics Letters 80 (2002) 1667–1669.
[17] S.S. Kim, S.I. Na, J. Jo, D.Y. Kim, Y.C. Nah, Plasmon enhanced performance of organic solar cells using electrodeposited Ag nanoparticles, Applied Physics Letters 93 (2008). (073307-1–073307-3).
[18] J.H. Lee, J.H. Park, J.S. Kim, D.Y. Lee, K. Cho, High efficiency polymer solar cells with wet deposited plasmonic gold nanodots, Organic Electronics 10 (2009) 416–420.
[19] S. Lal, S. Link, N.J. Halas, Nano-optics from sensing to waveguiding, Nature Photonics 1 (2007) 641–648.
[20] E. Hutter, J.H. Fendler, Exploitation of localized surface plasmon resonance, Advanced Materials 16 (2004) 1685–1706.
[21] D. Qi, M. Fischbein, M. Drndic, S. Selmic, Efficient polymer-nanocrystal quantum-dot photodetectors, Applied Physics Letters 86 (2005). (093103-1–093103-3).
[22] W.J.E. Beek, M.M. Wienk, M. Kemerink, X. Yang, R.A.J. Janssen, Hybrid zinc oxide conjugated polymer bulk heterojunction solar cells, Journal of Physical Chemistry B 109 (2005) 9505–9516.
[23] J. Weickert, R.B. Dunbar, H.C. Hesse, W. Wiedemann, Nanostructured organic and hybrid solar cells, Advanced Materials 23 (2011) 1810–1828.
[24] F.C. Chen, J.L. Wu, C.L. Lee, Y. Hong, C.H. Kuo, M.H. Huang, Plasmonic-enhanced polymer photovoltaic devices incorporating solution-processable metal nanoparticles, Applied Physics Letters 95 (2009). (013305-1–013305-3).
[25] C.C. Chang, H.L. Wu, C.H. Kuo, M.H. Huang, Hydrothermal synthesis of monodispersed octahedral gold nanocrystals with five different size ranges and their self-assembled structures, Chemistry of Materials 20 (2008) 7570–7574.
[26] J.Y. Kim, J.H. Jung, D.E. Lee, J. Joo, Enhancement of electrical conductivity of poly(3,4-ethylenedioxythiophene)/poly(4-styrenesulfonate) by a change of solvents, Synthetic Metals 126 (2002) 311–316.
[27] C.S. Lee, J.Y. Kim, D.E. Lee, Y.K. Koo, J. Joo, S. Han, Y.W. Beag., S.K. Koh, Organic based flexible speaker through enhanced conductivity of PEDOT/PSS with various solvents, Synthetic Metals 135–136 (2003) 13–14.
[28] S. Jeong, Y. Kwon, B.D. Choi, H. Ade, Y.S. Han, Improved efficiency of bulk heterojunction poly(3-hexylthiophene):[6,6]-phenyl-C_{61}-butyric acid methyl ester photovoltaic devices using discotic liquid crystal additives, Applied Physics Letters 96 (2010). (183305-1–183305-3).
[29] Y. Zhang, P.W.M. Blom, Electron and hole transport in poly(fluorene-benzothiadiazole), Applied Physics Letters 98 (2011). (143504-1–143504-3).
[30] T.Y. Chu, O.K. Song, Hole mobility of N,N′-bis(naphthalene-1-yl)-N,N′-bis(phenyl) benzidine investigated using space-charge-limited currents, Applied Physics Letters 90 (2007). (203512-1–203512-3).